DOI: 10.1002/ejic.200801068

Transformation of Solid Potassium Ferrate(VI) (K_2FeO_4): Mechanism and Kinetic Effect of Air Humidity

Libor Machala,[a] Radek Zboril,*[a] Virender K. Sharma,[b] Jan Filip,[a] Dalibor Jancik,[a] and Zoltan Homonnay[c]

Keywords: Solid-state reactions / Iron / Reaction mechanisms / Environmental chemistry / Moessbauer spectroscopy

The kinetics of solid-state transformation (aging) of potassium ferrate(VI) (K_2FeO_4) under various air-humidity conditions (55–95 % relative humidity) at room temperature were studied by in-situ Mössbauer spectroscopy. The kinetic data showed a significant increase in the decomposition rate with increasing air humidity. The decomposition kinetics is very unusual with two almost linear decay steps. The first slow decay was observable at rather lower humidity levels (55–70 %) probably due to the formation of the narrow compact layer of nanoparticulate $Fe(OH)_3$ reaction product. This layer limits the access of both H_2O and CO_2 participating in the reaction as the gaseous reactants. The second decay with much faster rate showed a nearly positive linear relationship with the humidity. The identification and characterization of the final products of aging were conducted by using X-ray diffraction (XRD), variable-temperature and in-field Mössbauer spectroscopy, magnetic measurements, thermogravimetry (TG) and differential scanning calorimetry (DSC), and scanning electron microscopy (SEM) techniques. The reaction mechanism, assuming formation of $KHCO_3$ and $Fe(OH)_3$ in the molar ratio of 2:1 per 1 mol of solid K_2FeO_4 was suggested. The SEM images revealed the formation of large $KHCO_3$ crystallites whose surface was covered by ultrasmall X-ray amorphous iron(III) hydroxide nanoparticles in a high degree of agglomeration. The obtained results of aging under humid conditions are important for the possible storage of K_2FeO_4 and thus for its environmental and industrial applications.

Introduction

Iron(VI) compounds [ferrates(VI), FeO_4^{2-}] represent an advanced class of compounds, which can be used in many promising electrochemical, environmental, and chemical applications such as high-energy-density rechargeable batteries[1–5] and cleaner ("greener") technologies of organic syntheses,[6–8] "environmentally friendly" oxidant useful in innovative technologies for water treatment.[9–24] Among multitudes of other advantageous properties it is worth to emphasize the coagulation and disinfection effects.[11,12,25–28]

The wide range of applications induced a great effort to prepare ferrate(VI) of sufficient purity on a large scale. Up to now, several synthetic routes were developed including chemical, electrochemical, and thermal techniques.[29–35] Regardless of the synthetic route, ferrate(VI) salts are relatively stable over a long period of time if stored in a dry atmosphere. However, they become quite unstable if treated at high temperatures[36] and/or if exposed to air humidity even at room temperature.[37]

The decomposition mechanism and stability of hexavalent iron compounds have been investigated in solutions,[4,38–42] whereas the solid-state room-temperature transformation has been reported only by Nowik et al.[37] The authors studied the disintegrations of solid K_2FeO_4 and $BaFeO_4$ samples sealed and exposed to dry and/or humid air. Mössbauer spectroscopy was applied to identify the possible intermediate oxidation states (V, IV) of iron and to characterize the final iron-bearing products.[37] In the case of K_2FeO_4, the final formation of Fe_2O_3 nanoparticles was suggested in both atmospheres, and no intermediates containing iron in higher valence states were detected. The potassium-containing reaction product has not been determined at all.[37]

The detailed analytical approach used in this paper provides evidence of the formation of $KHCO_3$ and amorphous $Fe(OH)_3$ as the aging products (molar ratio of 2:1) of K_2FeO_4 in humid air. This newly suggested reaction mechanism, assuming participation of the H_2O and CO_2 gaseous reactants, fills a gap in basic inorganic chemistry of high

[a] Centre for Nanomaterial Research and Departments of Experimental Physics and Physical Chemistry, Palacky University in Olomouc,
Svobody 26, 77146 Olomouc, Czech Republic
Fax: +420-58-563-4958
E-mail: zboril@prfnw.upol.cz
[b] Chemistry Department, Florida Institute of Technology, 150 West University Boulevard, Melbourne, Florida 32901, USA
[c] Department of Nuclear Chemistry, Eötvös Loránd University, Pázmány P. s. 1/A, 1117 Budapest, Hungary
Supporting information for this article is available on the WWW under http://www.eurjic.org or from the author.

oxidation states of iron. To the best of our knowledge, this is the first study on the kinetics of K_2FeO_4 aging under different humidity levels by in-situ Mössbauer spectroscopy to prove a drastic effect of relative air humidity on the aging rate. The two-step kinetics with an anomalous first slow stage is quantified and discussed in terms of the morphological and size changes of solid phases in the reaction system.

Results and Discussion

Kinetics of the K_2FeO_4 Aging

The kinetics of K_2FeO_4 aging was monitored by in-situ Mössbauer spectroscopy under different relative air-humidity conditions. Within the time interval $<t-1,t>$, where t is the aging time in hours, the relative content of ferrate(VI) was determined from the differential Mössbauer spectrum representing a difference in the spectra recorded at time t and at time $t-1$. As a result, under particular relative air-humidity conditions, the kinetics of K_2FeO_4 aging can be expressed as a time dependence of the relative spectrum area corresponding to the ferrate(VI) singlet subspectrum. In all three sets of spectra measured at a particular relative humidity, the singlet spectral component of the starting ferrate(VI) (δ_{Fe} = –0.88 to –0.92 mm/s; the range of isomer shift values corresponds well to those previously reported for K_2FeO_4[36,43–44]) gradually decreased in intensity with aging time. Simultaneously, the intensity of the doublet subspectrum (δ_{Fe} = 0.34–0.39 mm/s, ΔE_Q = 0.61–0.68 mm/s), corresponding to the high-spin iron(III) aging product, increased. No other spectral components have been detected during the collection of the spectra. This fact excludes the formation of any Fe^{IV} and Fe^{V} intermediates within the time scale of the measurement. The final Fe^{III} phase remains stable at room temperature under the set humidity conditions as confirmed by negligible changes in hyperfine parameters of the doublet subspectrum. For illustration, Figure 1 represents a typical Mössbauer spectrum recorded between the 6th and 7th hour of the aging at a relative air humidity (*RH*) of 65–70%. It is worthwhile to mention that a paramagnetic doublet with similar hyperfine parameters was observed in the ex-situ Mössbauer spectrum of a thermal decomposition product of K_2FeO_4 in air.[45] However, this doublet can be ascribed rather to an iron(III) oxide phase formed by aging of $KFeO_2$, which is primarily formed by thermal decomposition of K_2FeO_4.

The kinetic curves of K_2FeO_4 aging under different humidity conditions are shown in Figure 2A and B. It is worth to mention that the area of the singlet subspectrum does not represent the real weight content of the starting ferrate(VI) at the appropriate time. The corresponding molecular weights and Mössbauer *f*-factors[46] should be considered to recalculate the number of iron atoms corresponding to Fe^{VI} (singlet spectrum area) to the weight content of K_2FeO_4 in the reaction mixture. Nevertheless, such mathematical transformations are linear, so it is thus not necessary to take them into account for monitoring the effect of the relative air humidity on the kinetics of the K_2FeO_4 aging.

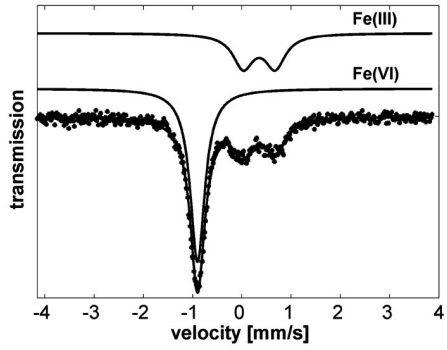

Figure 1. Room-temperature Mössbauer spectrum recorded between the 6th and 7th hour of the in-situ measurement (*RH* = 65–70%) starting from the potassium ferrate(VI) sample.

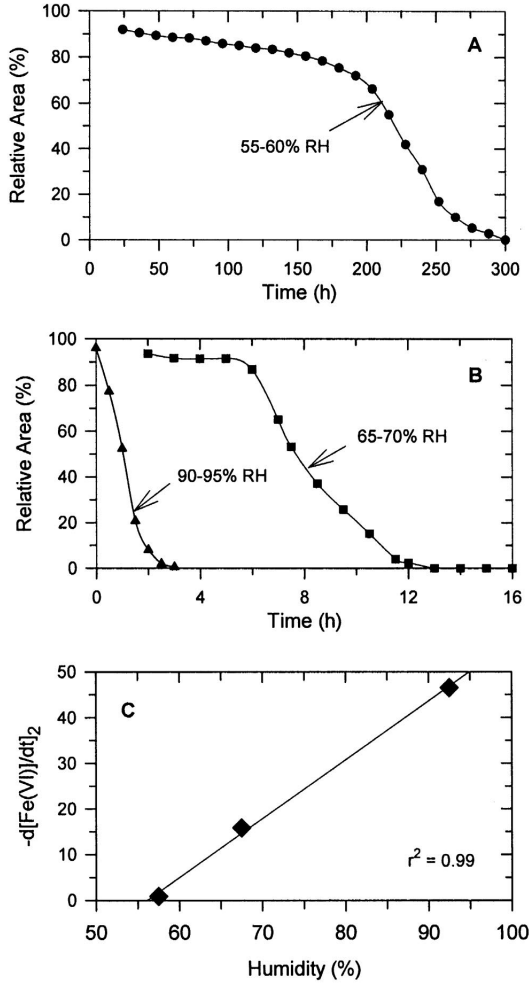

Figure 2. Kinetics of K_2FeO_4 aging expressed as dependence of Mössbauer spectral area on the relative humidity (A: lowest *RH*; B: higher *RH* levels; C: dependence of the second step decay rate on the relative humidity).

Figure 2 A and B show a strong influence of the relative air humidity on the aging kinetics of K_2FeO_4. Clearly, a faster transformation of K_2FeO_4 was observed with increasing humidity. Interestingly, kinetics of the decomposition reaction changed from the order of hours ($RH > 65\%$) to the order of days ($RH < 60\%$) (compare Figure 2A and B). For example, the complete decomposition of K_2FeO_4 took 12 h at RH = 65–70%, whereas the same conversion of Fe^{VI} to Fe^{III} took 12 d at RH = 55–60% (Figure 2).

At relative humidities of 55–60% and 65–70% (Figure 2A and B), we registered extraordinarily interesting kinetics as the decomposition of K_2FeO_4 occurred in two almost linear decays. The primary slow decay is truly linear and is followed by the second significantly faster decay, the main part of which (up to ca. 10% of Fe^{VI} in the reaction system) is also linear. The first slow decay was not seen at a high humidity of RH = 90–95% (Figure 2B). This fact manifests the key role of concentration of water as a gaseous reactant on the qualitative and quantitative character of the reaction kinetics. If a linear approximation is used for the evaluation of the second decay kinetics, a linear relationship between decay rate and humidity was obtained (Figure 2C). The linear relationship for a second step may be expressed as Equation (1). The standard deviations for the slope and the intercept have been determined as 0.0591 and 4.37, respectively.

$$-[d[Fe^{VI}]/dt]_2 = -72.43 + 1.2895 \times RH \quad (1)$$

Thus, the experimental data clearly demonstrate the dependence of both decays on the relative humidity, i.e. on the concentration of the water in the reaction system. With higher concentration of water a faster contact with solid K_2FeO_4 crystals can be expected. With higher relative humidity the primary decay takes place for a shorter time, and at highest humidity it even disappears. The explanation of the first slow stage and the abrupt change in reaction kinetics in the second fast step are strongly related to the reaction mechanism and to the morphological evolution of reaction products. Both will be discussed in detail in the next chapters.

Aging Mechanism, Characterization of Decomposition Products

To gain a better insight into the chemical, structural, and magnetic properties of the aging products, the decomposing sample under RH = 65–70% humid conditions at 12 h was subjected for detailed identifications and characterization. A label Fe^{VI}-12 was assigned to this sample, in which Fe^{VI} was almost fully transformed into the Fe^{III} phase (see Figure 2B). The XRD pattern of the sample reveals exclusively the lines of $KHCO_3$ as the only crystalline phase (Figure 3). Clearly, the Fe^{III} phase is X-ray-amorphous with a broad ridge in the 2θ range of 30–45°.

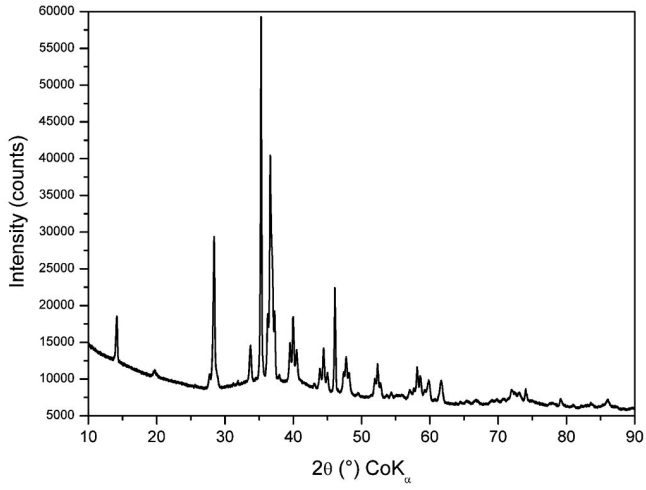

Figure 3. XRD pattern of the K_2FeO_4 sample aged for 12 h at RH = 65–70%. All detected diffraction lines can be ascribed to $KHCO_3$, PDF card no. 01-089-2369.

The temperature-dependent and in-field Mössbauer spectra of the Fe^{VI}-12 sample are shown in Figure 4. From the temperature evolution of the spectra, a blocking temperature obtained is ca. 50 K. The magnetically ordered sextet component dominates in the spectrum below 50 K. Such a low value of the blocking temperature indirectly confirms nanoparticle character of the iron-containing phase. In-field Mössbauer spectrum [Figure 4 (right)] exhibits practically unchanged intensities of the second and fifth spectral lines compared to the zero-field spectrum (3:2:1:1:2:3), which supports the speromagnetic behavior of the Fe phase.[46] This special kind of magnetic ordering is characteristic for amorphous iron oxides and hydroxides.[47]

Whereas Mössbauer spectroscopy brings information on the local magnetic ordering, macroscopic magnetic properties can be better monitored by SQUID magnetization measurements. Hysteresis loops of the Fe^{VI}-12 sample recorded at 10 and 300 K (Figure 5) did not saturate even at high external magnetic field (7 T), which is typically found for speromagnetic materials.[48] A magnetization curve at room temperature did not show any hysteresis, whereas a relatively low value of the coercive field (ca. 600 Oe) was observed at 10 K, below the magnetic transition temperature of the Fe^{III} phase. The maximum value of the magnetization determined at the highest applied magnetic field (H = 7 T) is 3.7 emu/g at room temperature. This value can be used as an important identification marker, mainly after its recalculation according to the weight percentage of the Fe^{III} phase in the mixture with $KHCO_3$. This will be further discussed in the text, after the determination of the chemical composition of the Fe^{III} phase.

The TG/DSC analyses of the aged Fe^{VI}-12 sample were conducted to determine the chemical composition of X-ray amorphous speromagnetic Fe^{III} phase and also to confirm the formation of $KHCO_3$ in the decomposition process (Figure 6). The DSC curve showed one broad endothermic effect (step I) between 25 and 100 °C corresponding evi-

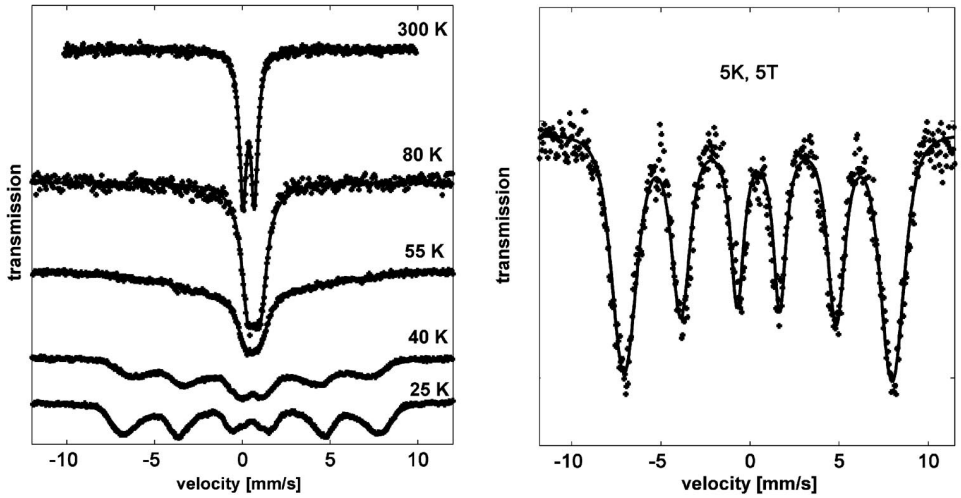

Figure 4. Temperature-dependent (left) and in-field (5 K, 5 T) Mössbauer spectra (right) of the K_2FeO_4 sample aged at room temperature for 12 h.

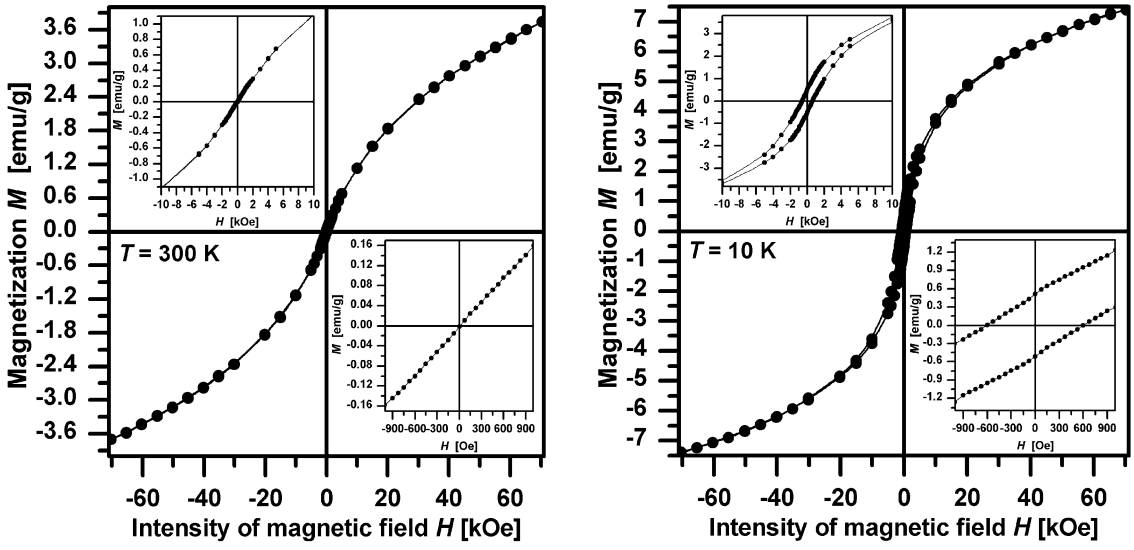

Figure 5. *M* vs. *H* magnetization curves (with two zooms) of the Fe^{VI}-12 sample recorded at 300 K (left) and 10 K (right).

dently to the evolution of the adsorbed gases and two other overlapping endothermic effects in the temperature range from 110 to 180 °C (step II), related to the decomposition of $KHCO_3$. For comparison, the inset of Figure 6 (left) shows the part of the DTA record measured on a pure $KHCO_3$ sample. A broad endothermic effect of the DSC curve between 100 and 186 °C was also observed during the decomposition of $KHCO_3$ by Lee et al.[49] The broad endothermic effect would be related to the broad size distribution of $KHCO_3$ crystals decomposing at different temperatures. Above 180 °C (step III), there was another broad endothermic effect, which could be ascribed to the transformation of the Fe^{III} phase. Analyzing the data regarding thermal stability of iron(III) oxides and oxy-hydroxides, all Fe_2O_3 polymorphs were excluded because they are thermally stable (and/or undergoing exothermic polymorphous transitions).

Additionally, Mössbauer spectra obtained in the present study are different from known spectra of all crystalline FeOOH and Fe_2O_3 polymorphs, except for δ-FeOOH, γ-FeOOH and β-Fe_2O_3. However, the formation of these phases can be excluded taking into account the found weight loss in the TG curve. Thus, the endothermic effect III above 180 °C could be explained solely by a gradual decomposition of iron(III) hydroxide [$Fe(OH)_3$] to iron(III) oxide.[50] The assignment of the Fe^{III} phase to $Fe(OH)_3$ explains its amorphous and speromagnetic nature originally determined by XRD, Mössbauer, and magnetic measure-

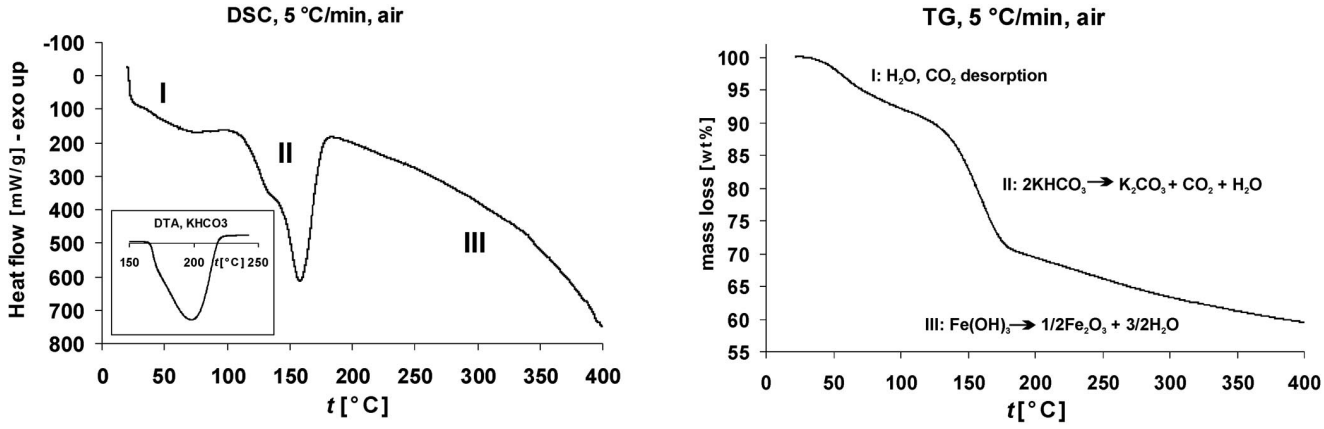

Figure 6. DSC (left) and TG (right) curves of the Fe^{VI}-12 sample measured in air (temperature step of 5 °C/min). The endothermic effects I, II, and III on the DSC curve correspond to the processes indicated in the TG curve. The inset shows endothermic effects measured on a pure $KHCO_3$ sample.

ments in the decomposition of K_2FeO_4 in humid air. Moreover, considering the starting atomic ratio of potassium/iron (2:1), $KHCO_3$ and $Fe(OH)_3$ should be formed in a molar ratio of 2:1 according to Equation (2).

$$K_2FeO_4 + 2\ CO_2 + 5/2\ H_2O \rightarrow 2\ KHCO_3 + Fe(OH)_3 + 3/4\ O_2 \quad (2)$$

The overall mass loss of 30 wt.-% determined between 110 and 400 °C from the TG curve of the Fe^{VI}-12 sample transformation is in good agreement with the theoretical value (29 wt.-%) calculated for decompositions of 2 $KHCO_3$ to K_2CO_3 and of $Fe(OH)_3$ to 1/2 Fe_2O_3 according to Equations (3) and (4).

$$2\ KHCO_3 \rightarrow K_2CO_3 + CO_2 + H_2O \quad (3)$$

$$Fe(OH)_3 \rightarrow 1/2\ Fe_2O_3 + 3/2\ H_2O \quad (4)$$

Both these decomposition steps are probably partially overlapped, and the decomposition of $Fe(OH)_3$ clearly dominates at higher temperatures [see the step assignments in Figure 6, right]. In summary, a room-temperature transformation of potassium ferrate(VI) in humid air containing water and carbon dioxide resulted in the formation of $KHCO_3$ and $Fe(OH)_3$ in a molar ratio of 2:1 with the simultaneous evolution of 3/4 mol of oxygen [Equation (2)].

Taking into account the molar ratio of $KHCO_3$/$Fe(OH)_3$ (2:1), the maximum value of the magnetization (at T = 10 K) was recalculated to 1 g of the $Fe(OH)_3$ phase. The value obtained was 21.5 emu/g, which corresponds well to reported magnetic data on amorphous iron(III) hydroxide.[50] This is a definite proof of the $Fe(OH)_3$ formation as the Fe^{III}-bearing reaction product. Other known iron(III) oxides such as antiferromagnetic hematite and goethite and/or ferrimagnetic maghemite and magnetite give significantly lower and/or considerably higher values of saturation magnetization.

The Size and Morphological Changes During K_2FeO_4 Aging

The changes in surface properties and morphologies of the starting ferrate(VI) and its solid transformation products [$KHCO_3$ and $Fe(OH)_3$] were investigated during the sample aging at a relative humidity of 65–70% by scanning electron microscopy (SEM) including energy-dispersive X-ray spectroscopy (EDX) and XRD.

Four representative samples were prepared at RH = 65–70% in order to describe accordingly both steps of the kinetic curve (see Figure 2B): (i) sample **A** (7% of Fe^{III}) – the very beginning of the first slow kinetic step; (ii) sample **B** (12%) – the end of the first slow kinetic step; (iii) sample **C** (27%) the very beginning of the second fast kinetic step; (iv) sample **D** – (98%, corresponds to Fe^{VI}-12) – the end of the aging process. The stage of sample transformation was directly checked by Mössbauer spectroscopy and expressed through the relative spectral area of the Fe^{III} phase (percentage values).

In the sample **A**, there are clearly observable well defined crystals of the starting K_2FeO_4 phase (2–10 μm) covered by some thin film corresponding probably to the primary reaction products, which form such a narrow amorphous layer on the ferrate(VI) surface (Figure 7A). This hypothesis agrees well with the fact that both reaction products, including $KHCO_3$ and $Fe(OH)_3$, are X-ray-amorphous at the very beginning of the ferrate(VI) transformation as their diffraction lines are not detected in the corresponding XRD pattern (see Figure 8). This surface layer is probably responsible for the slow first nearly linear kinetic step, as it prevents further access of gaseous reactants (H_2O, CO_2) for some time. With increasing time during the sample aging, small crystals of $KHCO_3$ (< 100 nm) appear, which gradually crystallize and thus break the homogeneity of the surface layer (Figure 7B). At some critical time, the growing $KHCO_3$ crystals cause cracks in the surface layer (see inset in Figure 7). This is probably of primary importance for further massive penetration of gaseous reactants towards

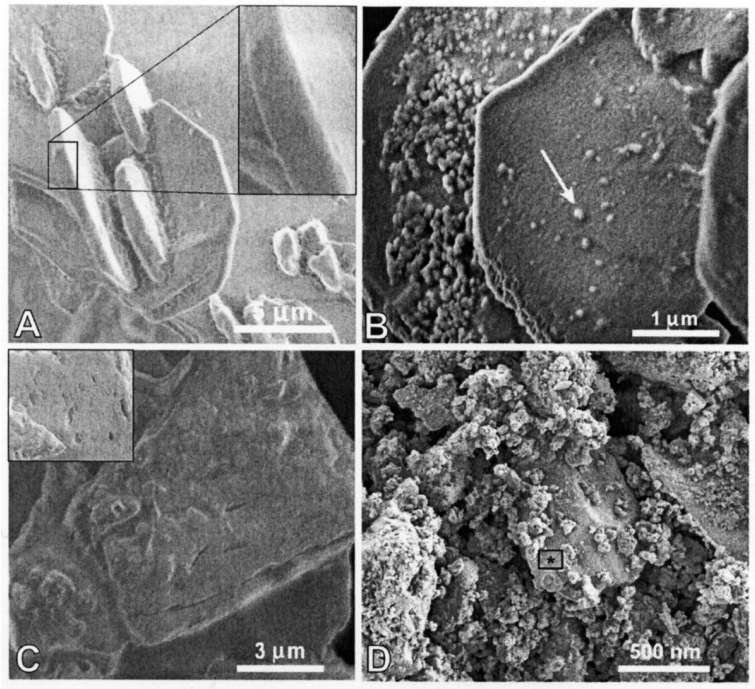

Figure 7. SEM images of a potassium ferrate(VI) sample aged up to different transformation stages at RH = 65–70%. A: very beginning of transformation (7% of Fe^{III}), B: end of the first slow kinetic step of (12% of Fe^{III}); the white arrow indicates one of the crystals of $KHCO_3$; C: beginning of the second fast kinetic step (27% of Fe^{III}); the inset demonstrates the presence of cracks in the selected region of the sample surface; D: end of the transformation (98% of Fe^{III}, sample Fe^{VI}-12); EDX analysis made from the area indicated by the black rectangle proved the presence of $KHCO_3$.

the ferrate(VI) crystal, which is reflected by the significant acceleration of the ferrate(VI) transformation. Finally, after the completion of the reaction process, relatively large crystallites of $KHCO_3$ (1 µm) are formed, and their surface is capped by iron(III) hydroxide nanoparticles in a high degree of agglomeration (Figure 7D). The EDX analysis of the free surface of the crystal (black rectangle in Figure 7D) confirms the chemical composition expected for the $KHCO_3$ with negligible content of iron (Supporting Information).

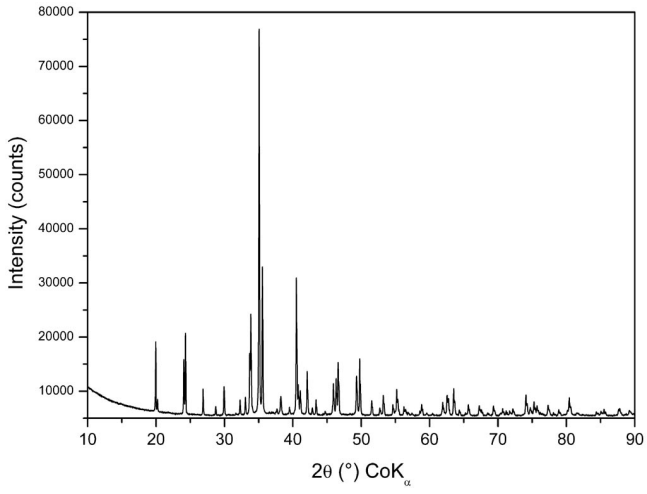

Figure 8. XRD pattern of the sample A prepared by short-time aging of potassium ferrate(VI) (7% of Fe^{III}). All diffraction lines are assignable to the starting ferrate(VI), a fact that indices the amorphous nature of the $KHCO_3$ and $Fe(OH)_3$ reaction products at the primary reaction stage.

To confirm the chemical nature of the crystals growing on the surface of a ferrate(VI) crystal and being probably responsible for the change in the reaction kinetics, we measured the EDX analysis (the line profile) of sample C, when the second fast reaction steps starts. As a result, we registered a considerable increase in the carbon and oxygen contents in the crystal on the surface of the starting ferrate(VI) (Figure 9). This analysis proves that the observed crystal corresponds to $KHCO_3$.

Conclusions

(i) In-situ Mössbauer measurements were applied for studying the K_2FeO_4 aging under various humid conditions. The decomposition rate of solid K_2FeO_4 changed from the order of hours at higher *RH* (65–95%) to the order of days at lower *RH* (55–60%), which is an important conclusion from the viewpoint of the practical use of ferrate(VI).

(ii) At lower humidity levels (55–70%), we observed anomalous two-step kinetics of the ferrate(VI) transformation, with the first nearly linear slow step followed by the second significantly faster step, the beginning of which is dependent on the relative humidity. We interpret this two-stage kinetics by the formation of a narrow amorphous layer of the reaction products on the surface of the fer-

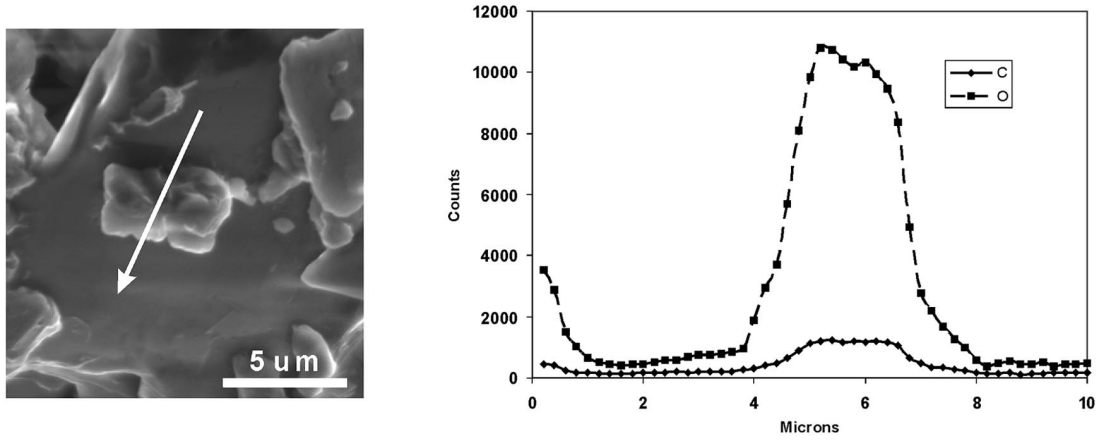

Figure 9. SEM image of sample C (27% of Fe^{III}) (left); EDX profile measured in the direction of the white arrow demonstrating a significant increase of carbon and oxygen in the area of the $KHCO_3$ crystal.

rate(VI) crystal. This layer probably prevents the access of gaseous reactants to the ferrate(VI) crystal for some time. The key role in the change of the reaction kinetics plays the crystallization of the hygroscopic $KHCO_3$ causing probably destruction of the layer and allowing thus the massive access of water and carbon dioxide to the reaction system.

(iii) X-ray analysis and Mössbauer spectroscopy revealed $KHCO_3$ and an amorphous Fe^{III} phase as the reaction products. For the first time, an iron(III) phase was unambiguously identified as nanoparticulate $Fe(OH)_3$ based on the results of structural, magnetic, and thermal analyses. The SEM images of the final reaction products show large (0.5–5 μm) crystallites of $KHCO_3$, which are covered by agglomerates of ultrasmall $Fe(OH)_3$ nanoparticles (< 10 nm). The formation of amorphous $Fe(OH)_3$ nanoparticles with large surface area suggests that this aging product of K_2FeO_4 may be even advantageous for removing contaminants through co-precipitation/adsorption processes.

Experimental Section

Sample Preparation: A powdered K_2FeO_4 sample (1–30 μm grain size) was prepared according to a method of Thompson et al.[29] Briefly, oxidation of $Fe(NO_3)_3{\cdot}9H_2O$ (Sigma–Aldrich) by hypochlorite in a strong NaOH solution resulted in sodium ferrate(VI) (Na_2FeO_4), which was then precipitated as potassium ferrate(VI) (K_2FeO_4) by adding KOH. The prepared crystals were then dried in ethanol and stored in a vacuum desiccator. The purity of the K_2FeO_4 sample was > 98%, confirmed by XRD and Mössbauer spectroscopic techniques.

Experimental Techniques: The transmission ^{57}Fe Mössbauer spectra were measured by using a Mössbauer spectrometer in a constant acceleration mode with a $^{57}Co(Rh)$ source. The isomer shift values were related to metallic α-iron at room temperature (r.t.). The measurements were carried out at various temperatures ranging from 25 to 300 K in a zero external magnetic field and at 5 K in an external magnetic field of 5 T, applied parallel to the direction of the γ-ray propagation. Low-temperature and in-field measurements were conducted by using a cryomagnetic system of Oxford Instruments. In-situ variable-air-humidity Mössbauer spectra were recorded by exposing the measured sample to flowing air (flow rate of 220 L/h) with different levels of relative humidity (*RH* = 55–60, 65–70, and 90–95%). For this purpose, the powdered sample was spread on glass wool and put into a conventional sample holder of the Mössbauer apparatus. The specially designed cell with uniformly distributed small holes was connected to a tube with flowing humid air (Figure 10). Mössbauer spectra were collected every hour to monitor the kinetics of the chemical transformation of potassium ferrate(VI). X-ray powder diffraction experiments were performed with a PANalytical X'Pert PRO instrument (Co-K_α radiation) equipped with an X'Celerator detector. Samples were placed on a zero-background Si slide, gently pressed in order to obtain a sample thickness of about 0.5 mm and scanned in the 2θ range of 10–90° in steps of 0.017°. A superconducting quantum interference device (SQUID, Magnetic Properties Measurement System –

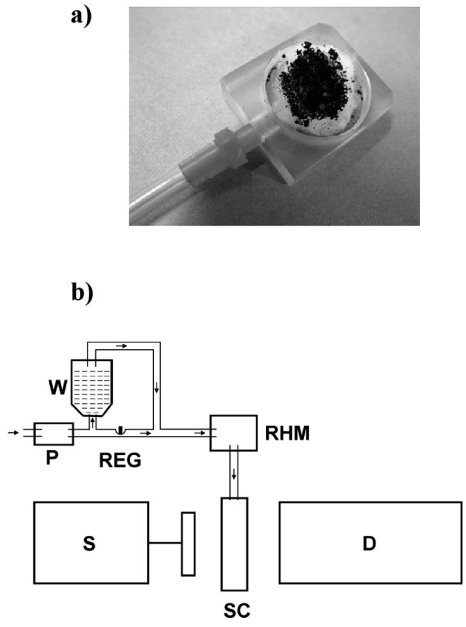

Figure 10. Sample cell (a) and schematic representation of the apparatus for the in-situ variable-air-humidity Mössbauer measurements (b); P: pump; REG: regulator for ambient air flow; W: bottle with water; RHM: sensor for measuring of the relative air humidity; SC: plastic sample cell; S: transducer with the radioactive source; D: scintillation detector.

MPMS XL-7, Quantum Design) was used for the magnetic measurements. The hysteresis loops were collected at 10 and 300 K in external magnetic fields of up to 7 T. Thermal behavior of the aging products was studied in static air by differential scanning calorimetry (DSC) and thermogravimetry (TG) by using a THASS XP-10 thermal analyzer at a heating rate of 5 °C/min. SEM images were obtained with a field-emission scanning electron microscope (SU6600, Hitachi) working at 3 kV.

Supporting Information (see footnote on the first page of this article): Energy-dispersive X-ray spectroscopy (EDX) analysis of the free surface of $KHCO_3$ crystal, which confirms the chemical composition.

Acknowledgments

Financial supports from the Ministry of Education of the Czech Republic (MSM6198959218, 1M6198959201, MEB040806) and from the Academy of Sciences of Czech Republic (KAN115600801) are gratefully acknowledged. The authors thank Jiri Frydrych and Jana Sevcikova (both from Palacky University, Czech Republic) for technical assistance, Jiri Tucek (Palacky University, Czech Republic) for magnetic measurements, and Janos Madarasz (Budapest University of Technology and Economics, Hungary) and Ria Yngard (Florida Institute of Technology) for useful discussion of the results.

[1] S. Licht, B. H. Wang, S. Ghosh, *Science* **1999**, *285*, 1039–1042.
[2] S. Licht, C. De Alwis, *J. Phys. Chem. B* **2006**, *110*, 12394–12403.
[3] K. A. Walz, A. N. Suyama, W. E. Suyama, J. J. Sene, W. A. Zeltner, E. M. Armacanqui, A. J. Roszkowski, M. A. Anderson, *Power Sources* **2004**, *134*, 318–323.
[4] K. E. Ayers, N. C. White, *J. Electrochem. Soc.* **2005**, *152*, A467–A473.
[5] S. Licht, V. Naschitz, B. H. Wang, *J. Power Sources* **2002**, *109*, 67–70.
[6] L. Delaude, P. Laszlo, *J. Org. Chem.* **1996**, *61*, 6360–6370.
[7] L. Delaude, P. Laszlo, P. Lehance, *Tetrahedron Lett.* **1995**, *36*, 8505–8508.
[8] V. K. Sharma, S. K. Mishra, N. Nesnas, *Environ. Sci. Technol.* **2006**, *40*, 7222–7227.
[9] V. K. Sharma, *Water Sci. Technol.* **2004**, *49*, 69–74.
[10] V. K. Sharma, *Adv. Environ. Res.* **2002**, *6*, 143–156.
[11] R. Yngard, S. Damrongsiri, K. Osathaphan, V. K. Sharma, *Chemosphere* **2007**, *69*, 729–735.
[12] V. K. Sharma, C. R. Burnett, R. Yngard, D. E. Cabello, *Environ. Sci. Technol.* **2005**, *39*, 3849–3854.
[13] V. K. Sharma, P. K. Dutta, A. K. Ray, *J. Environ. Sci. Health., Part A* **2007**, *42*, 997–1004.
[14] S. Z. Liu, B. H. Wang, B. C. Cui, L. L. Sun, *Fuel* **2008**, *87*, 422–428.
[15] H. Huang, D. Sommerfield, B. C. Dunn, E. M. Erying, C. R. Lloyd, *J. Phys. Chem. A* **2001**, *105*, 3536–3541.
[16] M. D. Johnson, J. F. Read, *Inorg. Chem.* **1996**, *35*, 6795–6799.
[17] V. K. Sharma, B. H. J. Bielski, *Inorg. Chem.* **1991**, *30*, 4306–4310.
[18] M. D. Johnson, B. J. Hornstein, *Inorg. Chem.* **2003**, *42*, 6923–6928.
[19] M. D. Johnson, B. J. Hornstein, *Chem. Commun.* **1996**, *8*, 965–966.
[20] T. Kamachi, T. Kouno, K. Yoshizawa, *J. Org. Chem.* **2005**, *70*, 4380–4388.
[21] Y. Shiota, N. Kihara, T. Kamachi, K. Yoshizawa, *J. Org. Chem.* **2003**, *68*, 3958–3965.
[22] H. Huang, D. Sommerfeld, B. C. Dunn, C. R. Lloyd, E. M. Eyring, *J. Chem. Soc., Dalton Trans.* **2001**, *8*, 1301–1305.
[23] Y. Lee, J. Yoon, U. V. Gunten, *Environ. Sci. Technol.* **2005**, *39*, 8978–8984.
[24] Y. Lee, B. I. Escher, U. V. Gunten, *Environ. Sci. Technol.* **2008**, *42*, 6333–6339.
[25] R. Yngard, V. K. Sharma, J. Filip, R. Zboril, *Environ. Sci. Technol.* **2008**, *42*, 3005–3010.
[26] Y. Lee, I.-H. Um, J. Yoon, *Environ. Sci. Technol.* **2002**, *37*, 5750–5756.
[27] P. Sylvester, L. A. Rutherford Jr, A. Gonzalez-Martin, J. Kim, B. M. Rapko, G. J. Lumetta, *Environ. Sci. Technol.* **2001**, *35*, 216–222.
[28] V. K. Sharma, *Water Sci. Technol.* **2007**, *55*, 225–230.
[29] G. W. Thompson, L. T. Ockerman, J. M. Schreyer, *J. Am. Chem. Soc.* **1951**, *73*, 1379–1381.
[30] J. M. Schreyer, G. W. Thompson, L. T. Ockerman, *Inorg. Synth.* **1953**, *4*, 164–168.
[31] K. Bouzek, M. J. Schmidt, A. A. Wragg, *Collect. Czech. Chem. Commun.* **2000**, *65*, 133–140.
[32] V. Lescuras-Darrou, F. Lapicque, G. Valentin, *J. Appl. Electrochem.* **2002**, *32*, 57–63.
[33] Y. M. Kiselev, N. S. Kopelev, N. A. Zavyalova, Y. D. Perfiliev, P. E. Kazin, *Zh. Neorg. Khim.* **1989**, *34*, 2199–2202.
[34] Y. D. Perfiliev, E. M. Benko, D. A. Pankratov, V. K. Sharma, *Inorg. Chim. Acta* **2007**, *360*, 2789–2791.
[35] S. Licht, X. Yu, in *Ferrate: Synthesis, Properties, and Applications in Water and Wastewater Treatment* (Ed.: V. K. Sharma), ACS Symposium Series, **2008**, vol. 985, pp. 1–45.
[36] L. Machala, R. Zboril, V. K. Sharma, J. Filip, O. Schneeweiss, Z. Homonnay, *J. Phys. Chem. B* **2007**, *111*, 4280–4286.
[37] I. Nowik, R. H. Herber, M. Koltypin, D. Aurbach, S. Licht, *J. Phys. Chem. Solids* **2005**, *66*, 1307–1313.
[38] C. Li, X. Z. Li, N. Graham, *Chemosphere* **2005**, *61*, 537–543.
[39] K. A. Walz, J. R. Szczech, A. N. Suyama, W. E. Suyama, L. C. Stoiber, W. A. Zeltner, M. E. Armacanqui, M. A. Anderson, *J. Electrochem. Soc.* **2006**, *153*, A1102-A1107.
[40] W. H. Yang, J. M. Wang, J. L. Cao, T. Pan, J. Q. Zhang, C. N. Cao, *Acta Chim. Sin.* **2004**, *62*, 1951–1955.
[41] S. Licht, V. Naschitz, B. Liu, S. Ghosh, N. Halperin, L. Halperin, D. Rozen, *J. Power Sources* **2001**, *99*, 7–14.
[42] K. Bouzek, M. J. Schmidt, A. A. Wragg, *J. Chem. Technol. Biotechnol.* **1999**, *74*, 1188–1194.
[43] R. H. Herber, D. Johnson, *Inorg. Chem.* **1979**, *18*, 2786–2790.
[44] S. K. Dedushenko, Y. D. Perfiliev, M. G. Goldfeld, A. I. Tsapin, *Hyperfine Interact.* **2001**, *136/137*, 373–377.
[45] T. Ichida, *Bull. Chem. Soc. Jpn.* **1973**, *46*, 79–82.
[46] E. Murad, H. Johnston, *Mössbauer Spectroscopy Applied to Inorganic Chemistry*, Plenum, New York, **1987**.
[47] L. Machala, R. Zboril, A. Gedanken, *J. Phys. Chem. B* **2007**, *111*, 4003–4018.
[48] E. Tronc, A. Ezzir, R. Cherkaoui, C. Chaneac, M. Nogues, H. Kachkachi, D. Fiorani, A. M. Testa, J. M. Greneche, J. P. Jolivet, *J. Magn. Magn. Mater.* **2000**, *221*, 63–79.
[49] K. S. Lee, I. W. Kim, *J. Phys. Soc. Jpn.* **2001**, *70*, 3581–3584.
[50] R. Cornell, U. Schwertmann, *The iron oxides: Structure, properties, reactions, occurrences, and uses*, Wiley-VCH GmbH & Co. KGaA, Weinheim, Germany, **2003**.

Received: October 31, 2008
Published Online: February 6, 2009

